Bull. Nov. Comp. Center, Comp. Science, 36 (2014), 103–113

Cellular automata simulation of self-organization in the bacterial MinCDE system*

Anton Vitvitsky

Abstract. The MinCDE protein complex is present in *Escherichia coli* and some other bacteria. *In vivo*, the MinCDE prevents incorrect cell division. *In vitro*, the MinCDE forms the protein waves and some other patterns. Recently, a hypothesis has been proposed, which says that *self-organization in the MinCDE system arises from an interplay of two opposing mechanisms*: *cooperative binding of MinD to the membrane, and accelerated MinD detachment due to persistent MinE rebinding.* On the basis of this hypothesis we have developed a cellular automaton model of the MinDE self-organization. A graph of the protein concentration, obtained as a result of computer simulations, reveals similarity with the graphs from the experiments *in vitro*. In addition, the visualization of computational experiments has shown propagating protein waves similar to those that emerge *in vitro*.

1. Introduction

The bacterial cell division begins with forming of a ring-like structure on the cell membrane in the midcell (Figure 1). This ring called Z-ring, consists of FtsZ polymers (tubulin-like protein) and is a framework for downstream cell division proteins [1]. A proper position of Z-ring in the midcell is controlled by certain self-organization mechanisms. Incorrect functioning of these mechanisms on mutant cells brings about invalid division and, subsequently, the mutants death [2]. A bright example of these self-organization mechanisms is a MinCDE protein complex, which is present in *Escherichia coli*. Currently, the processes leading to self-organization in this MinCDE system are not quite clear, but intensively being studied [3, 4].

The exact theoretical description of self-organization processes in biological systems is a hard task because of the difficulty to obtain information about spatio-temporal dynamics of individual particles from the bulk of biochemical assays. Hence, the computer simulation in this area plays an important role and helps in confirming (or disproving) the hypotheses proposed. Currently, one of the most effective tools of the discrete simulation of self-organization are Cellular Automata (CA). The cellular-automata models have the following advantages: the ability to simulate complex nonlinear processes in active environments, simple rules of simulation, spatialtemporal discreteness, easy visualization and natural fine-grained parallelism allowing

*Supported by RFBR under Grant 14-01-31425 mol_a.

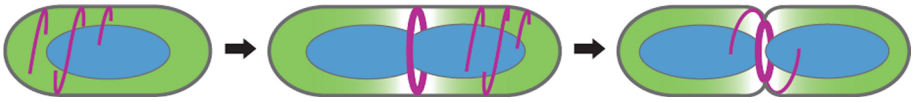

Figure 1. The Z-ring assembles in the midcell, where the concentration of negative regulators of assembly is the lowest [1]

one to effectively perform computations on modern multiprocessor systems (clusters, GPU, etc.) [5].

In this paper, we propose the Cellular Automaton model of self-organization MinCDE system, simulating processes *in vitro*, and its software implementation. Currently, there are several papers dealing with detailed experimental studies of the protein dynamics MinCDE *in vitro* [3, 4]. The results of this computer simulation can be compared to those obtained from experiments *in vitro*, and hence, help in confirming (or disproving) some existing MinCDE theoretical propositions.

2. Self-organization in the bacterial MinCDE system

The MinCDE system consists of the following proteins: MinC, MinD and MinE [1]. MinD diffuses from the cytosol into the inner membrane and binds to it. This binding is ATP-dependent, i.e., requires the presence of ATP-nucleotides. Next, MinE and MinC begin attaching to membrane-bound MinD, also diffusing from the cytosol. However, MinE and MinC are unable to bind independently to the membrane; MinC is an inhibitor of FtsZ polymerization and, respectively, prevents Z-ring assembly in its presence. In [2], it was suggested that the inhibitory activity of MinC is multifold increased by the presence of MinD. MinE competes with MinC for binding to membrane-bound MinD and as a result, displaces MinC back into the cytosol. After that, MinE stimulates ATP-hydrolysis of MinD and together they leave the membrane. In [6, 7], it was found that the minimal structural unit of MinCDE proteins interaction is a dimer.

In vivo, MinCDE system forms an oscillation process. Oscillations begin with what MinD is concentrating on the membrane of one of cell poles and recruits MinC. Then, E-ring, consisting of MinE proteins, is formed on the edge of the highest MinD protein concentration near the midcell. E-ring, traveling from the midcell to a cell pole, displaces MinDC from the membrane and after this, it also detaches. Farther, MinD (and accordingly MinD) begins to concentrate at the opposite cell pole, and the process repeats. Thus, a weak concentration (averaged over time) of FtsZ-polymers inhibitor is kept in the midcell, allowing Z-ring assembly. In [8–10], it was found that one cycle of oscillation is approximately 40–60 seconds. Figure 2 shows sequential frames that reflect the oscillation of MinCDE proteins in

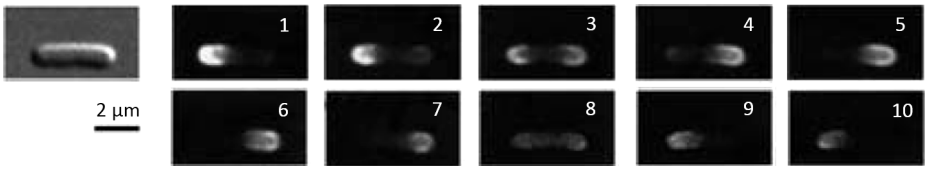

Figure 2. Time-lapse microscopy images of GFP-tagged MinD in *E. coli* [11]

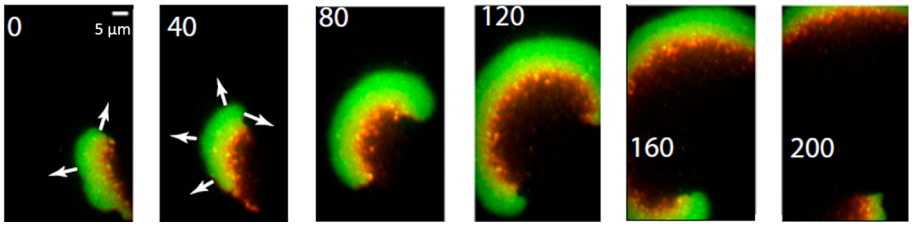

Figure 3. Waves on *E. coli* lipid bilayer [4]: MinD is green, MinE is red, the time stamps are in seconds, direction of wavefront propagation is labeled with arrows

E. coli. In [9], it was proposed that MinC does not affect the oscillation considered to be a passenger of MinDE.

In vitro, MinCDE system forms protein waves (Figure 3) and some other spatial-temporal patterns [4]. In [12], it was shown that MinD binds to the membrane cooperatively. However, there are no facts, confirming what MinD also cooperatively detaches from the membrane. Instead, in [3], it was proposed that MinE has the ability to rapidly rebind with the membrane-bound MinD, which means that MinE detaches from the membrane only when there are no other available MinD in the vicinity. As a result, MinE accumulates in the rear of a wave and stimulates ATP-hydrolysis that increases the rate of MinD detaching from the membrane. Thus, the theoretical model of MinCDE self-organization *in vitro* is as follows (Figure 4):

1. At the beginning of an oscillation cycle (or in the front of the protein wave) MinD-ATP starts to cooperatively bind to the membrane. Moreover, MinD diffuses on the membrane and periodically detaches back into solution, the latter being occurs without apparent signs of ATP-hydrolysis. With rising the MinD density, its residence time on the membrane is increased, and diffusion slows down. MinE from solution also starts to bind to the membrane-bound MinD, but in the beginning of an oscillation cycle the ratio of MinE/MinD is still too low and therefore protein detachment, due to ATP-hydrolysis, hardly occurs.

2. In the middle of an oscillation cycle (or in the middle of the wave), the ratio of MinE/MinD is increased, and,respectively, the protein detachment occurs more often. MinE continuously rebinds to the neighboring membrane-bound MinD.

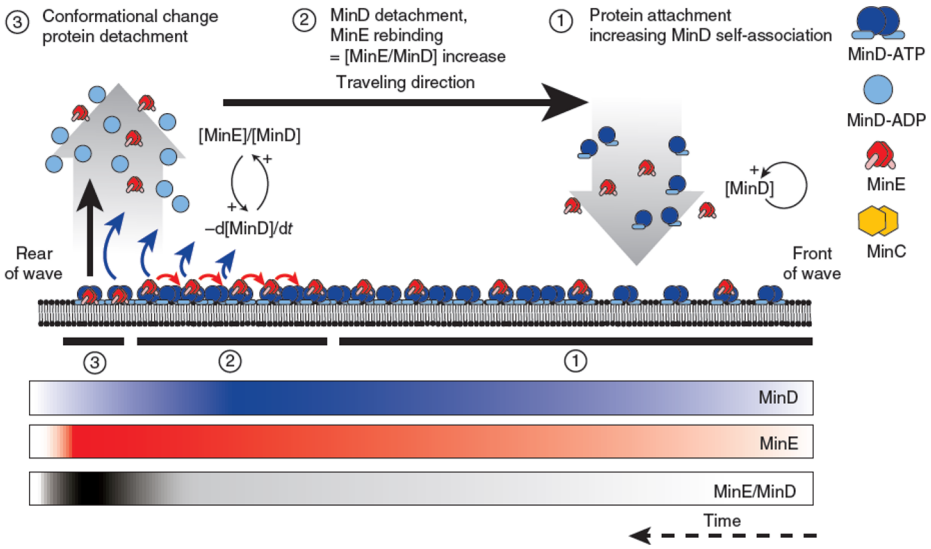

Figure 4. A model of Min-protein wave propagation. The figure is borrowed from [3]

3. At the end of an oscillation cycle (or in the rear of the wave), the ratio of MinE/MinD reaches its maximum, and MinE, interacting with the membrane, induces a conformational change, resulting in all MinC being displaced back into solution. Finally, MinE stimulates the bulk hydrolysis of MinD and all proteins rapidly disappear from the membrane.

3. Concepts and definitions of Cellular Automata

A cellular automaton (CA) is a discrete mathematical model consisting of a set of finite state automata called *cells* [13]. Each cell is defined by a pair $(u, \boldsymbol{x})$, where u is *a cell state* from the finite set of states A, and $\boldsymbol{x}$ is *a cell name* from the finite set of the name X. Cells located on a regular lattice and their set $\Omega = \{(u, \boldsymbol{x}) : \ u \in A, \ \boldsymbol{x} \in X\}$ form *a cellular array*. *Local configuration* $S(\boldsymbol{x}, t)$ is called a subset of cells in some neighborhood of the cell $(u, \boldsymbol{x})$ at the time t. More formally, $S(\boldsymbol{x}, t)$ is a multivalued function such that $S : X \to B$, where B is a family of subsets of the cellular array Ω.

Functioning of CA is defined using *the operator* Θ that determines the rules by which the cells $(u, \boldsymbol{x}) \in \Omega$ change their own states at the time t. Application of Θ to all $(u, \boldsymbol{x}) \in \Omega$ changes the global configuration $\Omega(t)$ to $\Omega(t+1)$. This change is called *iteration*. The operator Θ may consist of only one elementary substitution θ^{ρ} or superposition $\Theta = \Phi(\theta_1^{\rho}, \ldots, \theta_n^{\rho})$ [14]. Each substitution is applied to $\boldsymbol{x}$ according to its mode ρ and is defined as follows:

$$\theta_k^\rho: \quad S(\boldsymbol{x},t) \xrightarrow[[C]]{[P]} S(\boldsymbol{x},t+1),$$

where P are probability conditions for performing a substitution, that may be missing, C are other conditions that may also be missing.

The mode $\rho \in \{\alpha, \sigma\}$ defines the order of the substitution application to the cells. There are two basic modes: σ is *synchronous* and α is *asynchronous* one. In the synchronous mode, the operator Θ is applied to all the cells simultaneously: the new states of the cells are computed and then all the cells simultaneously change their own states to the new ones. In the asynchronous mode, the operator is applied to the cells one by one (in a random or a predetermined order): selecting a cell, computing its new state, changing its own state to the new one immediately. Hence, in the asynchronous mode one iteration consists of $|X|$ cycles.

More formally, a CA is defined by the triple $\mathfrak{B} = \langle A, X, \Theta\rangle$. Adding to this triple the initial global configuration, i.e., all the states of the cell array Ω at the time $t = 0$, forms a CA-model $\aleph = \langle \mathfrak{B}, \Omega(0)\rangle$.

4. The Cellular-Automata Model of MinDE Complex

The CA-model $\aleph_{\text{MinDE}} = \langle \mathfrak{B}, \Omega(0)\rangle$, presented here, simulates the self-organization process of MinDE proteins *in vitro*. The cells $(u, \boldsymbol{x}) \in \Omega$ are located in the nodes of a two-dimensional Cartesian lattice. The CA has a set of the names $X = \{\boldsymbol{x} : \ \boldsymbol{x}(i,j),\ i = 1,\dots,W,\ j = 1,\dots,H\}$, where $W \times H$ is the lattice size, and the set of states $A = \{\emptyset, \text{D}^{\text{ATP}}, \text{D}^{\text{ADP}}, \text{DE}^{\text{ATP}}, \text{DE}^{\text{ADP}}\}$, where $\emptyset$ means that a cell is "empty", and the remaining states correspond to the presence of one of MinD^{ATP}, MinD^{ADP}, $\text{MinDE}^{\text{ATP}}$, $\text{MinDE}^{\text{ADP}}$ proteins in the cell, respectively. At the initial time, all the cells $(u, \boldsymbol{x}) \in \Omega$ are set to $\emptyset$-state. The operator

$$\Theta = \Phi(\theta_1^\alpha, \theta_2^\alpha, \theta_3^\alpha, \theta_4^\alpha, \theta_5^\sigma, \theta_6^\sigma, \theta_7^\alpha)$$

determines the functioning of the model $\aleph_{\text{MinDE}}$.

Before considering the above substitutions in detail, let us introduce the following local configurations:

- Local configurations $S^1(\boldsymbol{x})$, $S^2(\boldsymbol{x})$, $S^3(\boldsymbol{x})$ are graphically represented in Figure 5: cells labeled as "1" belong to $S^1(\boldsymbol{x})$, those labeled as "2" — to $S^2(\boldsymbol{x})$, "3" — to $S^3(\boldsymbol{x})$.
- Local configuration $S_v^k(\boldsymbol{x}) \subseteq S^k(\boldsymbol{x})$ contains only those cells from $S^k(\boldsymbol{x})$ that are set to v-state.

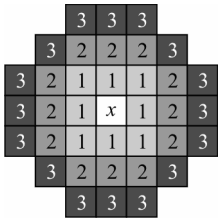

Figure 5

Now we consider the substitutions of the operator Θ in more detail:

$\boldsymbol{\theta_1^\alpha}$ is asynchronously applied. It simulates $\mathrm{MinD^{ATP}}$ binding to the membrane:

$$\theta_1^\alpha(\boldsymbol{x}): \ (\emptyset, \boldsymbol{x}) \xrightarrow[F_c(\boldsymbol{x})]{} (\mathrm{D^{ATP}}, \boldsymbol{x}),$$

An auxiliary function $F_c(\boldsymbol{x})$ reflects the cooperative membrane attachment:

$$F_c(x) = \begin{cases} 1, & \text{if rand} < P_1 + k_{11}|S^1_{\mathrm{D^{ATP}}}(\boldsymbol{x})| + k_{12}|S^2_{\mathrm{D^{ATP}}}(\boldsymbol{x})|, \\ 0, & \text{otherwise.} \end{cases}$$

where P_1 is probability of $\mathrm{MinD^{ATP}}$ binding to the membrane, k_{11} and k_{12} are coefficients reflecting the strength of the cooperative attraction $\mathrm{MinD^{ATP}}$ from the solution, $|S^1_{\mathrm{D^{ATP}}}(\boldsymbol{x})|$ and $|S^2_{\mathrm{D^{ATP}}}(\boldsymbol{x})|$ are the numbers of cells with D^{ATP} state from $S^1(\boldsymbol{x})$ and $S^2(\boldsymbol{x})$, respectively.

$\boldsymbol{\theta_2^\alpha}$ is asynchronously applied. It simulates membrane diffusion of $\mathrm{MinD^{ATP}}$ and $\mathrm{MinDE^{ATP}}$. The diffusion is presented by *naive diffusion* [15]:

$$\theta_2^\alpha(\boldsymbol{x}): \ \{(M_2, \boldsymbol{x}), (\emptyset, \boldsymbol{y})\} \xrightarrow[\text{rand}<k_2C_2]{P_2} \{(\emptyset, \boldsymbol{x}), (M_2, \boldsymbol{y})\},$$

where M_2 is any cell state from $\{\mathrm{D^{ATP}}, \mathrm{DE^{ATP}}\}$, $(\emptyset, \boldsymbol{y})$ is a randomly chosen "empty" cell from $S^1_\emptyset(\boldsymbol{x})$, P_2 is the diffusion coefficient [16,17], k_2 is the coefficient reflecting the strength of adhesion between MinD proteins preventing diffusion, $C_2 = |S^1_{\mathrm{D^{ATP}}}(\boldsymbol{x})| + |S^1_{\mathrm{DE^{ATP}}}(\boldsymbol{x})|$ is the number of cells with $\mathrm{D^{ATP}}$ or $\mathrm{DE^{ATP}}$ state from $S^1(\boldsymbol{x})$.

$\boldsymbol{\theta_3^\alpha}$ is asynchronously applied. It simulates the detachment of $\mathrm{MinD^{ATP}}$ and $\mathrm{MinDE^{ATP}}$ from the membrane:

$$\theta_3^\alpha(\boldsymbol{x}): \ (M_3, \boldsymbol{x}) \xrightarrow[\text{rand}<k_3C_3]{P_3} (\emptyset, \boldsymbol{x}),$$

where M_3 is any cell state from $\{\mathrm{D^{ATP}}, \mathrm{DE^{ATP}}\}$, P_3 is probability of the detachment of $\mathrm{MinD^{ATP}}$ or $\mathrm{MinDE^{ATP}}$ from the membrane, k_3 is the coefficient reflecting the strength of adhesion between $\mathrm{MinD^{ATP}}$ proteins preventing detachment, $C_3 = |S^1_{\mathrm{D^{ATP}}}(\boldsymbol{x})| + |S^1_{\mathrm{DE^{ATP}}}(\boldsymbol{x})|$ is the number of cells with $\mathrm{D^{ATP}}$ or $\mathrm{DE^{ATP}}$ state from $S^1(\boldsymbol{x})$.

$\boldsymbol{\theta_4^\alpha}$ is asynchronously applied. It is similar to the previous substitution, but for $\mathrm{MinD^{ADP}}$ and $\mathrm{MinDE^{ADP}}$:

$$\theta_4^\alpha(\boldsymbol{x}): \ (M_4, \boldsymbol{x}) \xrightarrow{P_4} (\emptyset, \boldsymbol{x}),$$

where M_4 is any cell state from $\{\mathrm{D^{ADP}}, \mathrm{DE^{ADP}}\}$, P_4 is probability of the detachment of $\mathrm{MinD^{ADP}}$ or $\mathrm{MinDE^{ADP}}$ from the membrane.

$\boldsymbol{\theta_5^\sigma}$ is synchronously applied. It simulates MinE binding to the membrane-bound $\mathrm{MinD}^{\mathrm{ATP}}$:

$$\theta_5^\sigma(\boldsymbol{x}): \ (\mathrm{D}^{\mathrm{ATP}}, \boldsymbol{x}) \xrightarrow{P_5} (\mathrm{DE}^{\mathrm{ATP}}, \boldsymbol{x}),$$

where P_5 is probability of MinE binding to $\mathrm{MinD}^{\mathrm{ATP}}$.

$\boldsymbol{\theta_6^\sigma}$ is synchronously applied. It simulates ATP hydrolysis by MinD stimulated via bound MinE:

$$\theta_6^\sigma(\boldsymbol{x}): \ (\mathrm{DE}^{\mathrm{ATP}}, \boldsymbol{x}) \xrightarrow{P_6} (\mathrm{DE}^{\mathrm{ADP}}, \boldsymbol{x}),$$

where P_6 is probability of the ATP hydrolysis by MinD.

$\boldsymbol{\theta_7^\alpha}$ is asynchronously applied. It simulates MinE rebinding to an available $\mathrm{MinD}^{\mathrm{ATP}}$:

$$\theta_7^\alpha(\boldsymbol{x}): \ \{(M_7, \boldsymbol{x}), (\mathrm{D}^{\mathrm{ATP}}, \boldsymbol{y})\} \xrightarrow[y \neq \emptyset]{P_7} \{(L_7, \boldsymbol{x}), (\mathrm{DE}^{\mathrm{ATP}}, \boldsymbol{y})\},$$

where M_7 is any cell state from $\{\mathrm{DE}^{\mathrm{ATP}}, \mathrm{DE}^{\mathrm{ADP}}\}$, L_7 is any cell state from $\{\mathrm{D}^{\mathrm{ATP}}, \mathrm{D}^{\mathrm{ADP}}\}$, P_7 is the probability of rebinding, $\boldsymbol{y} = F_r(\boldsymbol{x})$ is a cell with $\mathrm{MinD}^{\mathrm{ATP}}$-state chosen by the function $F_r(\boldsymbol{x})$:

$$F_r(\boldsymbol{x}) = \begin{cases} \mathrm{rand}(S^1_{\mathrm{D}^{\mathrm{ATP}}}(\boldsymbol{x})), & \text{if } n_1 \neq 0, \\ \mathrm{rand}(S^2_{\mathrm{D}^{\mathrm{ATP}}}(\boldsymbol{x})), & \text{if } n_1 = 0 \ \& \ n_2 \neq 0, \\ \mathrm{rand}(S^3_{\mathrm{D}^{\mathrm{ATP}}}(\boldsymbol{x})), & \text{if } n_1 = 0 \ \& \ n_2 = 0 \ \& \ n_3 \neq 0, \\ \emptyset, & \text{otherwise,} \end{cases}$$

where $n_1 = |S^1_{\mathrm{D}^{\mathrm{ATP}}}(\boldsymbol{x})|$, $n_2 = |S^2_{\mathrm{D}^{\mathrm{ATP}}}(\boldsymbol{x})|$, $n_3 = |S^3_{\mathrm{D}^{\mathrm{ATP}}}(\boldsymbol{x})|$.

5. Computer simulation results

To verify the developed model, a series of computational experiments has been carried out. The collected data resulting from the simulations are compared to the data obtained in the experiments *in vitro*. The model parameters of computational Experiments 1 and 2 were empirically chosen, so that the graph of protein concentration obtained as a result of computer simulations matches graphs from the experiments *in vitro*. The process of selecting the model parameters is a difficult task. To demonstrate the dependence of the model protein concentration of some parameters, Experiments 3 and 4 were performed.

Experiment 1 had the following model parameters:

- A rectangular lattice consisting of 200×200 cells that approximately corresponds to 1.6×1.6 µm.

- $P_1 = 0.00001$, $P_2 = 0.5$, $P_3 = 0.3$, $P_4 = 0.5$, $P_5 = 0.0004$, $P_6 = 0.03$, $P_7 = 1.0$.
- $k_{11} = 0.013$, $k_{12} = 0.00065$, $k_2 = 5.5$, $k_3 = 1.8$.

Figure 6 shows the comparison graphs of protein concentration by experiment 1 and *in vitro*. Let us note that in this comparison we are more interested in the similarity of the graphs character instead of their exact quantitative identity. A small peak before a decrease in the protein concentration in Figure 6a is caused by a conformational change of the MinDE-complex [3], which was not taken into account in our model.

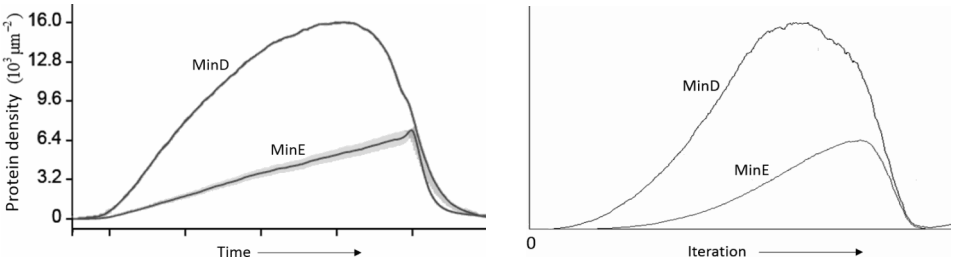

Figure 6. Protein surface densities with respect to time dependency: a) estimated surface densities of MinD and MinE *in vitro* (the figure is borrowed from [3]) and b) the result of computer simulation with Experiment 1

Experiment 2 was performed with the parameters of Experiment 1 except the lattice size being 175×300 cells that approximately corresponds to 1.58×2.4 µm. Figure 7 shows the visualization results in this case: MinD is shown in dark gray, MinE — in light gray. The snapshots with iterations numbers 341, 1,271 and 2,821 display a sequential process of MinD accumulation on the membrane (and, accordingly, MinE). Then, the ratio of MinD/MinE becomes critical and in the snapshots with iterations numbers 4,061 and 4,836 a propagating wave is observed. In the last snapshot with iteration number 7,905 the ongoing process of wave propagation is visible.

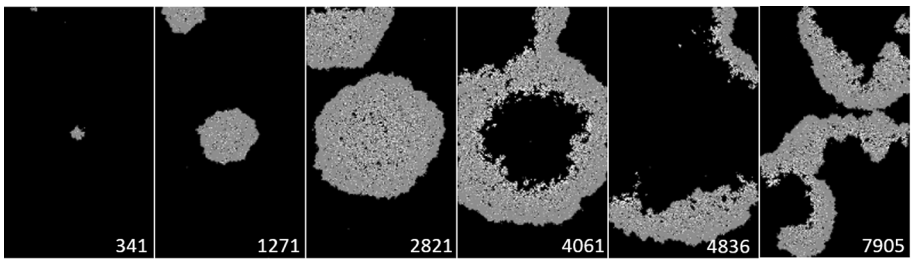

Figure 7. Experiment 2. Numbers denote the iteration numbers

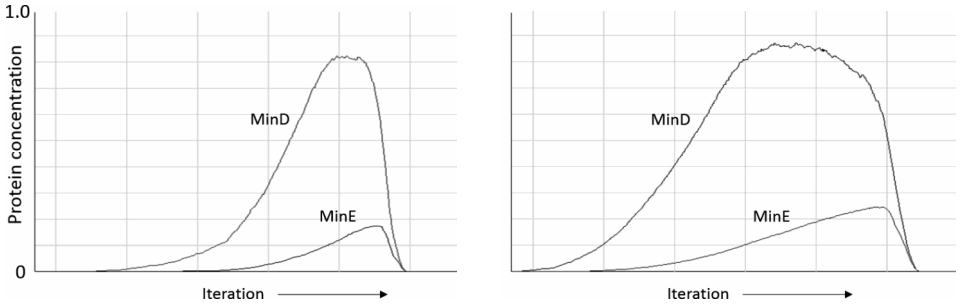

Figure 8. Protein surface densities simulated with a) Experiment 3 and b) Experiment 4

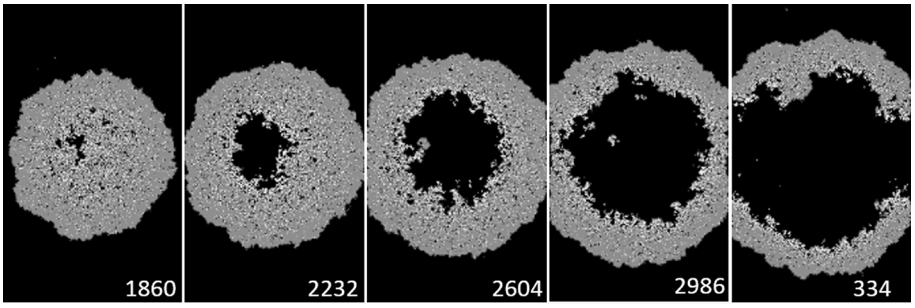

Figure 9. Emergence of a wave in Experiment 4. Numbers denote the iteration numbers

Moreover, in the snapshot with iteration number 4,061, a formed E-ring consisting of MinE proteins (of a lighter color) can be seen.

Experiments 3 and 4 were performed with the parameters of Experiment 1 except $P_5 = 0.0002$, $P_6 = 0.05$ for Experiment 3 and $P_6 = 0.04$ for Experiment 4. The results are shown in Figure 8. It is seen that the dependence of surface densities on time is deformed relative to those given in [3]. The snapshots taken in performing Experiment 4 are shown in Figure 9. The emergence of waves is also visible.

6. Conclusion

The CA-model of the self-organization MinDE protein complex based on the theoretical description from [3] has been developed. The graph of protein concentration, obtained as a result of computer simulations, has revealed the similarity with the graphs from the experiments *in vitro* from [3, 4]. In addition, the visualization of computational experiments has shown the propagation of protein waves similar to those that emerge *in vitro*.

Thus, the evidence in favor of the hypothesis from [3], which says that the *self-organization in the MinCDE system arises from an interplay of two opposing mechanisms*: *cooperative binding of MinD to the membrane, and accelerated MinD detachment due to persistent MinE rebinding* have been obtained.

References

[1] Lutkenhaus J. Assembly dynamics of the bacterial MinCDE system and spatial regulation of the Z ring // Annu. Rev. Biochem. — 2007. — Vol. 76. — P. 539–562.

[2] Fange D., Elf J.. Noise-induced Min phenotypes in E. coli // PLoS Comput. Biol. — 2006. — Vol. 2, No. 6. — e80; doi:10.1371/journal.pcbi.0020080.

[3] Loose M., Fischer-Friedrich E., Herold C., Kruse K., Schwille P. Min protein patterns emerge from rapid rebinding and membrane interaction of MinE // Nat. Struct. Mol. Biol. — 2011. — Vol. 18. — P. 577–583; doi:10.1038/nsmb.2037.

[4] Ivanov V., Mizuuchi K. Multiple modes of interconverting dynamic pattern formation by bacterial cell division proteins // Proc. Natl Acad. Sci. USA. — 2010. — Vol. 107. — P. 8071–8078.4.

[5] Bandman O. Implementation of large-scale cellular automata models on multi-core computers and clusters // High Performance Computing and Simulation (HPCS), 2013 Int. Conf / IEEE Conference Publications. — 2013. — P. 304–310.

[6] Lutkenhaus J., Sundaramoorthy M. MinD and role of the deviant Walker A motif, dimerization and membrane binding in oscillation // Mol. Microbiol. — 2003. — Vol. 48. — P. 295–303.

[7] Leonard T., Butler P.J., Lowe J. Bacterial chromosome segregation: structure and DNA binding of the Soj dimer — a conserved biological switch // EMBO J. — 2005. — Vol. 24. — P. 270–282.

[8] Hu Z., Lutkenhaus J. Topological regulation of cell division in Escherichia coli involves rapid pole to pole oscillation of the division inhibitor MinC under the control of MinD and MinE // Mol. Microbiol. — 1999. — Vol. 34. — P. 82–90.

[9] Raskin D.M., de Boer P.A.J. Rapid pole-to-pole oscillation of a protein required for directing division to the middle of Escherichia coli // Proc. Natl Acad. Sci. USA. — 1999. — Vol. 96. — P. 4971–4976.

[10] Fu X., Shih Y.-L., Zhang Y., Rothfield L.I. The MinE ring required for proper placement of the division site is a mobile structure that changes its cellular location during the Escherichia coli division cycle // Proc. Natl Acad. Sci. USA. — 2001. — Vol. 98. — P. 980–985.

[11] Hale C.A., Meinhardt H., de Boer P.A.J. Dynamic localization cycle of the cell division regulator MinE in Escherichia coli // EMBO J. — 2001. — Vol. 20. — P. 1563–1572.

[12] Lackner L., Raskin D., Boer P. ATP-dependent interactions between Escherichia coli Min proteins and the phospholipid membrane in vitro // J. Bacteriol. — 2003. — Vol. 185. — P. 735–749.

[13] Bandman O. Cellular automata composition techniques for spatial dynamics simulation // Simulating Complex Systems by Cellular Automata. Understanding Complex Systems / A.G. Hoekstra et al., eds. — Berlin: Springer, 2010. — P. 81–115.

[14] Achasova S., Bandman O., Markova V., Piskunov S. Parallel Substitution Algorithm. Theory and Application. — Singapore: World Scientific, 1994.

[15] Toffolli T., Margolus N. Cellular Automata Machines: A New Environment for Modeling. — USA: MIT Press, 1987.

[16] Bandman O. The concept of invariants in reaction-diffusion cellular-automata // Bull. Novosibirsk Comput. Center. Ser. Computer Science. — Novosibirsk, 2012. — Iss. 33. — P. 24–36.

[17] Medvedev Yu.G. Multiparticle cellular automata for diffusion simulation // MTPP Proc. — Berlin: Springer, 2011. — P. 204–211. — (LNCS; 6083).